Exact Distribution of the Quantal Content in Synaptic Transmission

Krishna Rijal,[1] Nicolas I. C. Müller,[2] Eckhard Friauf,[2] Abhyudai Singh,[3] Ashok Prasad,[4,*] and Dibyendu Das[1,†]
[1]Department of Physics, Indian Institute of Technology Bombay, Powai, Mumbai 400076, India
[2]Animal Physiology Group, Department of Biology, University of Kaiserslautern, Kaiserslautern, Germany
[3]Departments of Electrical and Computer Engineering, Biomedical Engineering and Mathematical Sciences, University of Delaware, Newark, Delaware 19716, USA
[4]Department of Chemical and Biological Engineering, Colorado State University, Fort Collins, Colorado, USA

(Received 19 July 2023; revised 26 January 2024; accepted 25 April 2024; published 31 May 2024; corrected 17 July 2024)

During electrochemical signal transmission through synapses, triggered by an action potential (AP), a stochastic number of synaptic vesicles (SVs), called the "quantal content," release neurotransmitters in the synaptic cleft. It is widely accepted that the quantal content probability distribution is a binomial based on the number of ready-release SVs in the presynaptic terminal. But the latter number itself fluctuates due to its stochastic replenishment, hence the actual distribution of quantal content is unknown. We show that exact distribution of quantal content can be derived for general stochastic AP inputs in the steady state. For fixed interval AP train, we prove that the distribution is a binomial, and corroborate our predictions by comparison with electrophysiological recordings from MNTB-LSO synapses of juvenile mice. For a Poisson train, we show that the distribution is nonbinomial. Moreover, we find exact moments of the quantal content in the Poisson and other general cases, which may be used to obtain the model parameters from experiments.

DOI: 10.1103/PhysRevLett.132.228401

The human brain is arguably the most complex natural object in the known universe. Its complexity, as well as its capabilities, are a product of its roughly 86×10^9 [1] neurons that make approximately 10^{15} connections [2] with each other. The majority of these connections are chemical synapses, a schematic diagram of which is shown in Fig. 1(a), with the vesicle-rich presynaptic terminal on the left and the postsynaptic terminal with neurotransmitter receptors on the right. In the presynaptic terminal, ready-release synaptic vesicles (SVs) packed with neurotransmitters attach to docking sites. The arrival of an action potential (AP) controls the calcium dynamics, which triggers the stochastic fusion of a few SVs (the "quantal content") with the presynaptic membrane, thereby releasing their neurotransmitter cargo in the synaptic cleft as shown. A stochastic train of APs is shown in Fig. 1(b) (top) and the corresponding time dependent quantal content is shown schematically (below). Experimentally the quantal content is obtained as the ratio of the measured peak amplitude of evoked (excitatory or inhibitory) postsynaptic currents [3] to average quantal size. Thus, SV release from presynaptic terminals is a fundamental feature of all information processing in the nervous system.

Addressing how neurons communicated with one another, Castillo and Katz [4] first proposed what they described as a quantal theory of release of certain binomially distributed "units." Over the years microstructural and electrophysiological studies revealed the relevant biological details, and a picture emerged of spatially distributed pools of neurotransmitters containing SVs in the presynaptic neuron. These are the resting, recycling, and ready-release pools (RRPs). SVs from the RRPs may release their neurotransmitter cargo on stimulation by an AP through membrane fusion at the presynaptic terminal [5–8]. Sustained APs require RRP replenishment, and early theoretical analysis assumed deterministic replenishment, and quantal release [9–11]. Later works developed probabilistic descriptions and stochastic models [12–18]. Empirical observations had shown that the binomial distribution

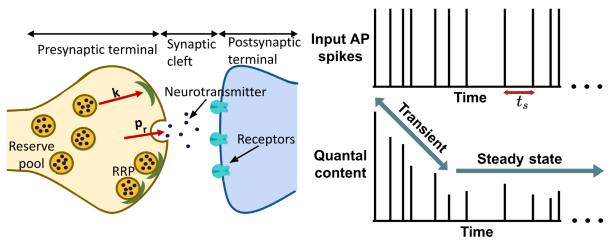

FIG. 1. (a) Schematic picture of a chemical synapse. The SVs (circular balls) filled with neurotransmitters (black dots) get docked to sites (in green) and remain ready to release at the presynaptic terminal. Each AP triggers release of some SVs to the synaptic cleft, which reach the receptors in postsynaptic terminal to produce evoked postsynaptic current. (b) A schematic input AP train with random intervals t_s (top), and (bottom) the output quantal content varying with time, shown to reach a steady state at long times.

was a good fit to the statistics of quantal release, and this has been the basis of the majority of fluctuation analysis [12,16,18–27]. The basic model thus assumes that at the instant of AP stimulation, if there are n_- docked SVs in RRPs and p_{r_t} is the instantaneous release probability, then quantal content b (fused and released SVs) is distributed as $B(n_-, p_{r_t}, b) = \binom{n_-}{b} p_{r_t}^b (1-p_{r_t})^{n_- - b}$ [16–18,24,28–30].

As n_- is itself stochastic, it is generally expected that the actual distribution of quantal content is not a binomial, as would result from summing over the likelihood of random values of n_-. This fact has largely been overlooked in the literature and some works even used binomial with n_- approximated by its mean value [16–18,28,29,31,32]. Systematic formalism treating the docked vesicle number stochastically appeared in a set of works [33–36], although the focus of the authors was the estimation of the model parameters. While exact relationships between probability of postsynaptic currents after two successive APs were formally written down, the problem could not be solved analytically further because of the presence of multiple nested summations due to the explicit history of the AP train [34].

In this Letter, we show that in the *steady state* limit after sustained AP stimulation, for uncorrelated stochastic interspike intervals (ISI), the full distribution of quantal content b as well as its moments becomes *analytically tractable*. The commonly used fixed ISI stimulation follows as a special case of our general result. Although the transient plastic regime [Fig. 1(b)] is often studied in synapses, the steady state is also of interest [7,16,24,37] and is attained in experimentally reasonable times [38,39]. Poisson AP stimulation has been experimentally studied [40], and such ISI distributions have been observed in visual cortical neurons [41,42]. Thus, stochastic stimulations are an important *in vivo* scenario. These facts provide motivation for our focus here on steady state quantal content under stochastic stimulations.

In Fig. 2, the time dependent number $n(t)$ of docked SVs in the presynaptic neuron is shown schematically. Starting with $n = n_{+,m-1}$ after the $(m-1)$th AP, the number grows stochastically to $n = n_{-,m}$ up to a time t_{s_m}, at which the appearance of the mth AP leads to the fusion and release of b_m vesicles, resulting in a sudden decrease of SVs from $n_{-,m} = n_{+,m} + b_m$ to $n_{+,m}$.

We assume that docked vesicles may be released probabilistically after an AP but do not otherwise detach. Following the empirical literature [16,17,24,28,30], as mentioned above, the distribution of b_m is $B(n_{-,m}, p_{r_t}, b_m) = \binom{n_{-,m}}{b_m} p_{r_t}^{b_m} (1-p_{r_t})^{n_{-,m}-b_m}$, where the release probability p_{r_t} is time dependent but saturates at long time. However, $n_{-,m}$ itself is stochastic and is replenished as follows. We assume M is the maximum number of available docking sites, and that docking sites are refilled from the vesicle pool at a rate proportional to the number of empty sites,

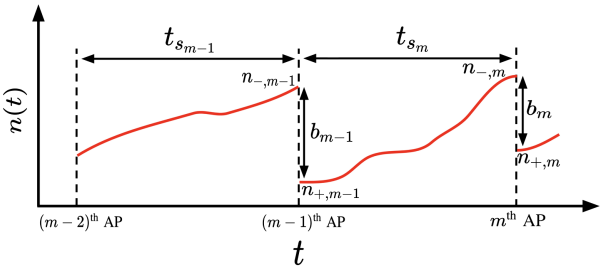

FIG. 2. The time variation of docked SV number $n(t)$ is shown as a function of time over two successive ISIs between the $m-2$ and $m-1$ and mth APs. The respective numbers before an AP (n_-) after an AP (n_+) and quantal content (b) are shown.

i.e., $k_t(M-n)$ [16,18], where k_t is the time dependent docking rate per empty site. The stochastic replenishment of docked SVs from an initial $n_{+,m-1}$ to some n in time t is described by the conditional distribution $p(n,t|n_{+,m-1})$.

Exact recursive relations may be written between the probabilities $P_+^m(n_{+,m}, t_{s_m})$ and $P_+^{m-1}(n_{+,m-1}, t_{s_{m-1}})$ for the SV numbers $n_{+,m}$ and $n_{+,m-1}$ after mth and $(m-1)$th AP respectively, similar to ideas in [33,34]:

$$P_+^m(n_{+,m}, t_{s_m}) = \sum_{n_{+,m-1}, b_m} B(n_{+,m}+b_m, p_{r_t}, b_m) \times p(n_{+,m}+b_m, t_{s_m}|n_{+,m-1}) \times P_+^{m-1}(n_{+,m-1}, t_{s_{m-1}}). \quad (1)$$

Similarly, the probability of SV number $n_{-,m}$ just prior to the mth AP, namely $P_-^m(n_{-,m}, t_{s_m})$, is given by

$$P_-^m(n_{-,m}, t_{s_m}) = \sum_{n_{+,m-1}} p(n_{-,m}, t_{s_m}|n_{+,m-1}) \times P_+^{m-1}(n_{+,m-1}, t_{s_{m-1}}). \quad (2)$$

The nested nature of the Eqs. (1) and (2) depending on the full history of successive ISIs make problems of these type analytically very challenging and various computational methods have been developed in this context [33,34,36]. In this Letter we focus on the long time limit after sustained AP stimulation, when interestingly we find that the problem becomes analytically tractable.

Whether the input stimulation is a deterministic AP train [39] or a stochastic one [40], on sustained stimulation (i.e., the index m of AP and time is large), a *steady state* [7,16,24,38,39] is expected to be reached. In this limit, the mean quantal content $\langle b \rangle$ becomes a constant, and its distribution $Q^{ss}(b)$ becomes time independent. Analytically obtaining $Q^{ss}(b)$ is the main aim of this work. Note that in this $t \to \infty$ limit, the time-varying calcium concentration-dependent replenishment rate k_t and release probability p_{r_t} saturates to constant values $k = k_\infty$ and $p_r = p_{r_\infty}$—see representative curves in Sec. 1 of the

Supplemental Material (SM) [43] following a model of Ref. [11], and the corresponding time varying $\langle b\rangle$ reaching a steady state. As we solely focus on the steady state, the only two neuronal model parameters we assume in our calculations are k and p_r. We will show that these can be estimated by comparing experimental data with exact moments of quantal content that we derive.

We study stochastic AP stimulations but assume that the ISIs are uncorrelated, i.e., the joint distribution of two intervals t_{s_m} and t_{s_n}, namely $g_2(t_{s_m}, t_{s_n}) = g(t_{s_m})g(t_{s_n})$. Under this assumption, for any general stochastic ISI distribution $g(t_s)$, in steady state, it may be shown (see Appendix A) that the Eqs. (1) and (2) become

$$P_+^{ss}(n_+) = \sum_{n'_+,b} \int_0^\infty dt_s g(t_s) B(n_+ + b, p_r, b) \times p(n_+ + b, t_s | n'_+) P_+^{ss}(n'_+) \quad (3)$$

$$P_-^{ss}(n_-) = \sum_{n'_+} \int_0^\infty p(n_-, t_s | n'_+) P_+^{ss}(n'_+) g(t_s) dt_s. \quad (4)$$

At long times, m is large. Therefore, we have used $n_{+,m-1} = n'_+$, $n_{+,m} = n_+$, $n_{-,m} = n_-$, and $b_m = b$ as they become history independent random variables. For the case of common experimental interest of fixed ISIs we need to set $g(t_s) = \delta(t_s - T)$. The conditional distribution $p(n, t|n'_+)$ for n'_+ to become n in time $t = t_s$, used in Eqs. (3) and (4), satisfy the master equation [44]

$$\frac{\partial p(n,t|n'_+)}{\partial t} = k[M-(n-1)]p(n-1,t|n'_+) - k[M-n]p(n,t|n'_+). \quad (5)$$

This equation can be solved using the generating function $F(q,t|n'_+) = \sum_n q^n p(n,t|n'_+)$ (see Appendix B for details), and the solution is

$$p(n,t|n'_+) = \binom{M-n'_+}{n-n'_+} (1-e^{-kt})^{n-n'_+} e^{-[k(M-n)]t}. \quad (6)$$

The true steady state distribution of quantal content $Q^{ss}(b)$ is obtained by summing its binomial distribution at every release step over all possible docked random SV numbers n_-,

$$Q^{ss}(b) = \sum_{n_-=0}^{M} B(n_-, p_r, b) P_-^{ss}(n_-). \quad (7)$$

Thus, to calculate $Q^{ss}(b)$, we need the steady state distribution $P_-^{ss}(n_-)$, and in turn $P_+^{ss}(n_+)$ because of the relationships in Eqs. (3) and (4). The Eq. (3) has $P_+^{ss}(n_+)$ on both sides. Through a lengthy calculation (see details in Sec. 2 of SM [43]), we show that the corresponding generating function, namely $F_+(q) = \sum_{n_+=0}^\infty q^{n_+} P_+^{ss}(n_+)$ can be obtained using the knowledge of $F(q,t|n'_+)$, the generating function for $p(n,t|n'_+)$ obtained in Eq. (B2). This generating function leads us to two other relevant generating functions, $F_-(q) = \sum_{n_-=0}^\infty q^{n_-} P_-^{ss}(n_-)$ and $F_b(q) = \sum_{b=0}^\infty q^b Q^{ss}(b)$, corresponding to the distributions $P_-^{ss}(n_-)$ and $Q^{ss}(b)$. Since the three stochastic variables, n_-, n_+, and b, are related to each other through the relationship $n_+ = n_- - b$, the different generating functions are also related (see details in Sec. 3 of SM [43]):

$$F_-(q) = F_+\left(\frac{q-p_r}{1-p_r}\right) \quad \text{and} \quad F_b(q) = F_+\left(\frac{p_r(q-1)}{1-p_r}+1\right). \quad (8)$$

Once we know $F_b(q)$, we may obtain the desired distribution $Q^{ss}(b)$ (see Sec. 3 of SM [43]) using the standard relationship $Q^{ss}(b) = (1/b!)[\partial^b F_b(q)/\partial q^b]|_{q=0}$ [44]:

$$Q^{ss}(b) = \sum_{n=0}^\infty \binom{n}{b} (-1)^{n-b} \binom{M}{n} \frac{p_r^n}{1-(1-p_r)^n L_n} \left[\phi_{n,0} + \sum_{\{S_{(n-1)}\}} \frac{(1-p_r)^{\sum_i m_i} \phi_{n,m_z}\phi_{m_z,m_{z-1}}\cdots\phi_{m_1,0}}{\prod_i (1-(1-p_r)^{m_i} L_{m_i})}\right], \quad (9)$$

where $\phi_{n,m} = \binom{n}{m}\int_0^\infty dt_s g(t_s) e^{-nkt_s}(e^{kt_s}-1)^{n-m}$ and $L_n = \int_0^\infty dt_s g(t_s) e^{-nkt_s}$.

In Eq. (9), $\{S_{(n-1)}\}$ denotes the set of all the subsets $S_{(n-1)} = \{m_i\} = (m_z, m_{z-1}, \ldots, m_1)$ with $m_i \in (1,2,\ldots,n-1)$ such that $m_z > m_{z-1} > \cdots > m_1$. Although the upper limit of the sum is shown up to ∞, due to the combinatorial factor $\binom{M}{n}$, n never exceeds M. Note that for an arbitrary $g(t_s)$ there is no reason to expect that $Q^{ss}(b)$ in Eq. (9) would reduce to a binomial distribution.

The closed form expressions of the mean and $CV^2 = (\langle b^2\rangle/\langle b\rangle^2) - 1$ of the distribution in Eq. (9) (see Sec. 3 in SM [43]) are

$$\langle b\rangle = \frac{M p_r \phi_{1,0}}{1-(1-p_r)L_1}, \quad \text{and}$$

$$CV^2 = \frac{\phi_{1,0} + p_r L_1}{M\phi_{1,0}} \left\{\frac{(M-1)}{1-(1-p_r)^2 L_2}\left[\phi_{2,0}\left(1+\frac{p_r L_1}{\phi_{1,0}}\right) + (1-p_r)\phi_{2,1}\right] + \frac{1}{p_r}\right\} - 1. \quad (10)$$

As fixed frequency trains are commonly used in experiments, and Poisson-like statistics have been observed in the ISI distribution from neurons in the visual cortex [41,42], explicit expressions of $Q^{ss}(b)$ in these two special cases are desirable. For constant ISI $t_s = T$, also called a fixed frequency $f = 1/T$ AP train, we have $g(t_s) = \delta(t_s - T)$.

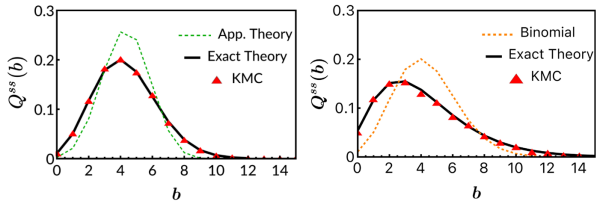

FIG. 3. Steady state quantal content distributions for (a) fixed AP arrival times ($f = 1/T = 20$ Hz), and (b) exponentially distributed ISIs (rate $f_0 = 20$ Hz). The common parameters are $M = 50$, $p_r = 0.5$, $k = 2$ s^{-1}. The exact theoretical curves (thick lines) match the KMC data (red symbols). In (a) an approximate (see text) binomial distribution (dashed line) is shown alongside the exact binomial. In (b) the binomial distribution of Eq. (11) with $T \to 1/f_0$ (dashed line) deviates from the exact nonbinomial distribution.

In Sec. 4(a) in SM [43], we shown that $Q^{ss}(b)$ in this case reduces to a binomial distribution,

$$Q^{ss}(b) = B(M, p_{rb}, b), \tag{11}$$

$$\text{where } p_{rb} = \frac{(1 - e^{-kT})p_r}{1 - (1 - p_r)e^{-kT}}. \tag{12}$$

The exact binomial distribution has the parameters M and a modified release probability p_{rb} given by Eq. (12), which depends on the interval T and growth rate k apart from p_r. We do kinetic Monte Carlo (KMC) simulations (Sec. 5 in SM [43]) to verify our analytical predictions. In Fig. 3(a), we see that the exact distribution $Q^{ss}(b)$ [Eq. (11)] matches perfectly the data from KMC simulations of this process (see the red symbols). Note that Eq. (11) is not equivalent to an approximate binomial often used in the literature $B(\langle n_- \rangle, p_r, b)$. In fact we calculate exactly $\langle n_- \rangle = Mp_{rb}/p_r$ [see Sec. 4(a) in SM [43]], and use this to plot $B(\langle n_- \rangle, p_r, b)$ (dashed line) in Fig. 3(a), which deviates significantly. In the large T limit, from Eq. (12), $p_{rb} \to p_r$ (the release probability in the steady state), as one would expect. The mean and CV^2 of b from Eq. (11) are

$$\langle b \rangle = Mp_{rb} \quad \text{and} \quad CV^2 = \frac{(1 - p_{rb})}{Mp_{rb}}, \tag{13}$$

For Poisson AP train, the ISIs are exponentially distributed with $g(t_s) = f_0 e^{-f_0 t_s}$. Obtaining $\phi_{n,m}$ and L_n in this case, Eq. (9) simplifies [see details in Sec. 4(b) in SM [43]] to yield the following quantal content distribution:

$$Q^{ss}(b) = \sum_{n=0}^{\infty} (-1)^{n-b} \frac{{}^nC_b\, {}^MC_n\, n!(kp_r)^n}{\prod_{i=1}^{n}(f_0 + ki - (1 - p_r)^i f_0)}. \tag{14}$$

The corresponding mean and CV^2 for the Poisson case [see Sec. 4(b) in SM [43]] are

$$\langle b \rangle = \frac{Mkp_r}{k + f_0 p_r} \quad \text{and}$$
$$CV^2 = \frac{1}{M}\left(\frac{2(M-1)(k + f_0 p_r)}{2k + f_0 p_r(2 - p_r)} + \frac{f_0}{k} - M + \frac{1}{p_r}\right). \tag{15}$$

Note that this distribution is no longer a binomial. In Fig. 3(b) we see that the exact formula (solid line) for $Q^{ss}(b)$ [Eq. (14)] matches very well with the data obtained from KMC simulation (in symbols). Just to demonstrate that a binomial approximation would be completely inadequate in this Poisson case, we plot Eq. (11) with $T = 1/f_0$ where f_0 is the Poisson rate—the deviation is stark. In real biological synapses, ISIs may have correlations, i.e., t_{s_m} may depend on previous t_{s_j} (with $j < m$). In Sec. 6 of SM [43], we study two models with correlated ISI using KMC, and show that for small correlations, the $Q^{ss}(b)$ do not deviate drastically from Eq. (14), implying its practical usefulness.

Experimental verification and estimation of model parameters.—We performed electrophysiological experiments in acute brainstem slices of juvenile mice (postnatal day 11) at MNTB-LSO synapses (see Appendix C-I). Neurons were stimulated with constant ISI at 100 Hz for 1 s. After 30 s rest period, this was repeated, and we collected data from 20 repeats. The quantal content was determined as the ratio of the peak amplitude of evoked inhibitory postsynaptic currents to the current produced by a single quantum (q) [pA/(pA/SV)]—details are in [45,46].

In Figs. 4(a) and 4(b), for two synapses (referred to as synapse-1 and synapse-2, respectively), we plot the time-varying fluctuating quantal contents for one history (in blue), and average over 20 repeats (in red). In both neurons the mean quantal content reaches a steady state value beyond 0.8 s (see the yellow box). Thus between times 0.8 and 1 s over 20 repeats, the sample size of quantal contents per synapse was 400, which were used to plot the experimental distributions (in green) in Figs. 4(c) and 4(d). We compare this with the theory in the following way.

After the first AP (at 0 s), the quantal content b_0 should follow a binomial distribution $B(M, p_{r_0}, b_0)$, since docking sites should have maximal occupancy. From the 20 experimental histories, the mean and variance of b_0 was compared with that of $B(M, p_{r_0}, b_0)$, to obtain M by eliminating p_{r_0}. Next we equate the experimental steady state $\langle b \rangle$ [Figs. 4(c) and 4(d)] to the theoretical mean $\langle b \rangle = Mp_{rb}$ [Eq. (13)], and determine the parameter p_{rb}. With these M and p_{rb}, we plot the theoretical distributions Eq. (11) for the two synapses against the experimental ones in Figs. 4(c) and 4(d). To assess how well the distributions match, the *Kullback-Leibler divergence* [47] was calculated to be 0.034 and 0.041 and the *mean squared error* was 0.00023 and 0.00013 for synapse-1 and 2, respectively (see

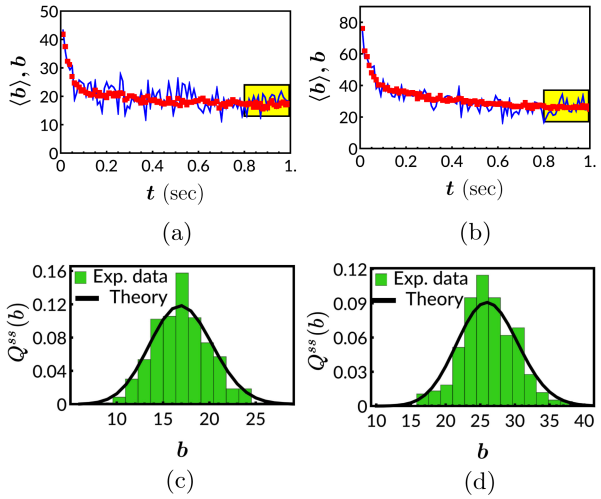

FIG. 4. The experimental mean quantal content $\langle b \rangle$ is plotted (in red) against time for (a) synapse-1 and (b) synapse-2. The blue curves represent one of the 20 experimental realizations of the quantal content. The yellow box shows the part of data we considered to be in the steady state for plotting the experimental histograms of quantal content in (c) and (d) (in green). In (c) and (d), the parameter values used for the exact theoretical distributions (black curves) for synapse-1 are $M = 50$ and $p_{rb} = 0.345$ and for the synapse-2 are $M = 98$ and $p_{rb} = 0.266$.

Appendix C-II). These low values show that the distributions match well, which is further corroborated by a comparison of moments (Appendix C-II). Such a comparative study of the full experimental and theoretical distributions is now also possible for stochastic inputs with Poisson APs (using Eq. (14) or any other $g(t_s)$ (using Eq. (9)) in future.

Note that the moments in the fixed ISI case depend on the composite parameter p_{rb} [Eq. (13)] and not separately on p_r and k, so we cannot estimate them using moments of the data. But if experimental data on frequency ($f = 1/T$) dependent $\langle b \rangle = M p_{rb}$ is available, and other parameters are known, then k may be estimated. Published experimental data in [39] gives $\langle b \rangle$ versus f, and kM and p_r, for three different neurons. By fitting Eq. (12) to the data in these three cases, we estimate the respective k values (see Appendix C-III).

For Poisson APs the model parameters p_r and k may be estimated by solving the theoretical moment formulas [Eq. (15)] equated to the experimental values. This may be done for any other ISI distributions $g(t_s)$ using Eq. (10). To demonstrate the feasibility of the procedure, we generate finite sized sample sets of quantal content through KMC with Poisson APs. Comparing moments of such simulated data with Eq. (15) we show (see Sec. 7 in SM [43]) that estimates of p_r and k converge reliably as the size of the sample set goes beyond a few hundred.

Exact results are rare and desirable in biological contexts. Here, we analyze the basic model of synaptic transmission between neurons applicable to all chemical synapses. For any uncorrelated stochastic AP input, in the steady state regime, we provide full exact general distributions including moments, and show how experimental data may be compared to theory and model parameters may be estimated. The basic model does not account for complexities revealed by recent research such as feedback effects [48,49], vesicle priming [50], and spatial heterogeneities [51,52]—incorporation of these in future must rest upon a thorough analysis of the basic model, which we have presented here.

D. D. acknowledges IIT Bombay for funding. K. R. thanks IIT Bombay for Institute Ph.D. fellowship. A. S. acknowledges support by NIH/NIDCD Grant No. R01DC019268. E. F. acknowledges support by Bundesministerium für Bildung und Forschung, FundRef ID. 01GQ2001, Title ModSynTrans.

Appendix A: Self-consistent equation for the quantal content distribution $P_+^{ss}(n_+)$ in the steady state.—In Eq. (1), the probability $P_+^m(n_{+,m}, t_{s_m})$ after the mth AP is related to $P_+^{m-1}(n_{+,m-1}, t_{s_{m-1}})$ after the $(m-1)$th AP, by summing over all paths that take $n_{+,m-1}$ to $n_{+,m}$. Each path involves the initial probability $P_+^{m-1}(n_{+,m-1}, t_{s_{m-1}})$, the probability $p(n_{+,m} + b, t_{s_m} | n_{+,m-1})$ for $n_{+,m-1}$ to rise to $n_{+,m} + b$ in time t_{s_m}, and finally the probability for the number $n_{+,m} + b$ of docked vesicles to reduce to $n_{+,m}$ by AP triggered vesicle release, with the associated quantal content $b_m = b$ distributed binomially as $B(n_{+,m}+b, p_r, b)$.

We may follow the same procedure for $P_+^{m-1}(n_{+,m-1}, t_{s_{m-1}})$ and so on, and build up a hierarchy of relations for any interval between two APs. The problem remains hard to solve as result for every interval depends on the history of the previous interval. We are particularly interested in the steady state attained after several APs appear, i.e., $m \gg 1$ and the output quantal contents statistically stabilize. We integrate Eq. (1) over the joint probability distribution $g_2(t_{s_m}, t_{s_{m-1}})$ of t_{s_m} and $t_{s_{m-1}}$. We get

$$\begin{aligned}
&\int_0^\infty \int_0^\infty dt_{s_m} dt_{s_{m-1}} g_2(t_{s_m}, t_{s_{m-1}}) P_+^m(n_{+,m}, t_{s_m}) \\
&= \int_0^\infty \int_0^\infty dt_{s_m} dt_{s_{m-1}} g_2(t_{s_m}, t_{s_{m-1}}) \\
&\quad \times \sum_{n_{+,m-1}, b} p(n_{+,m} + b, t_{s_m} | n_{+,m-1}) \\
&\quad \times B(n_{+,m} + b, p_r, b) P_+^{m-1}(n_{+,m-1}, t_{s_{m-1}}). \qquad \text{(A1)}
\end{aligned}$$

If the interspike intervals (ISIs) are not correlated, we would have $g_2(t_{s_m}, t_{s_{m-1}}) = g(t_{s_m}) g(t_{s_{m-1}})$, where $g(t_{s_m})$ and $g(t_{s_{m-1}})$ are the normalized distributions of t_{s_m} and $t_{s_{m-1}}$, respectively. Under this assumption,

$$\int_0^\infty \int_0^\infty dt_{s_m} dt_{s_{m-1}} g(t_{s_m}) g(t_{s_{m-1}}) P_+^m(n_{+,m}, t_{s_m})$$
$$= \int_0^\infty \int_0^\infty dt_{s_m} dt_{s_{m-1}} g(t_{s_m}) g(t_{s_{m-1}})$$
$$\times \sum_{n_{+,m-1},b} p(n_{+,m}+b, t_{s_m}|n_{+,m-1})$$
$$\times B(n_{+,m}+b, p_r, b) P_+^{m-1}(n_{+,m-1}, t_{s_{m-1}}). \quad \text{(A2)}$$

This further simplifies to

$$\int_0^\infty dt_{s_m} g(t_{s_m}) P_+^m(n_{+,m}, t_{s_m})$$
$$= \sum_{n_{+,m-1},b} \int_0^\infty dt_{s_m} g(t_{s_m})$$
$$\times p(n_{+,m}+b, t_{s_m}|n_{+,m-1}) B(n_{+,m}+b, p_r, b)$$
$$\times \int_0^\infty dt_{s_{m-1}} g(t_{s_{m-1}}) P_+^{m-1}(n_{+,m-1}, t_{s_{m-1}}). \quad \text{(A3)}$$

In the long time limit, the steady state probability distribution of the vesicle number $P_+^{ss}(n_+) = \int_0^\infty dt_{s_m} g(t_{s_m}) P_+^m(n_{+,m}, t_{s_m})$, independent of the exact history of the spike train. Dropping the subscripts m (in the steady state), and setting $t_{s_m} = t_s$ and $n_{+,m-1} = n'_+$, Eq. (A3) leads to Eq. (3).

Following similar line of reasoning, one may derive Eq. (4) from Eq. (2).

Appendix B: Probability distribution of docked vesicle number n between two consecutive action potentials.—In the interval t to $t+dt$, the number of docked vesicles increases from $n-1$ to n with the probability $k(M-(n-1))dt$, and hence the master equation for $p(n,t|n'_+)$ is given by Eq. (5). The generating function $F(q,t|n'_+) = \sum_n q^n p(n,t|n'_+)$, where $n'_+ \le n \le M$. Otherwise, $p(n,t|n'_+) = 0$ if n'_+ falls outside this range. Multiplying Eq. (5) by $\sum_n q^n$ on both sides, we get an equation for F:

$$\frac{\partial F}{\partial t} + kq(q-1)\frac{\partial F}{\partial q} = kM(q-1)F. \quad \text{(B1)}$$

Equation (B1) is solved by the method of Lagrange characteristics to yield

$$F(q,t|n'_+) = q^M \left[1 - \frac{(q-1)}{q} e^{-kt}\right]^{M-n'_+}. \quad \text{(B2)}$$

Doing a binomial expansion of Eq. (B2) and relabeling $n + n'_+ \to n$ we get

$$F = \sum_{n=n'_+}^{M} \binom{M-n'_+}{n-n'_+} q^n (1-e^{-kt})^{n-n'_+} (e^{-kt})^{M-n}. \quad \text{(B3)}$$

Then we compare Eq. (B3) with the definition of F and obtain $p(n,t|n'_+)$ as given by Eq. (6) in the text.

Appendix C: Details on our experiments, theory-experiment comparison, and comparison with published data.—I: The fast auditory MNTB-LSO synapses consist of inhibitory glycinergic inputs from the medial nucleus of the trapezoid body (MNTB) to neurons in the lateral superior olive (LSO) and are known for maintaining reliable interneuronal communication even during prolonged high-frequency stimulation [46,53]. We refer the reader to the Methods section of Ref. [46] for details on the slice preparation and details of whole-cell patch-clamp recordings. The stimulation protocol consisted of repetitive tetanic AP bursts (100 Hz, 1 s) that were given 20 times. A 30-s rest period was introduced between repeats to allow for recovery from short-term depression.

II: We now discuss how we compare the full experimental distribution of quantal content with that of our theory after matching their means. Denoting the experimental quantal content distribution as $Q^{\rm ex}(b)$ and given that the theoretical is $Q^{ss}(b)$, we use the *Kullback-Leibler divergence* (KL) as a measure of closeness of the two as $\mathrm{KL} = \sum_b Q^{ss}(b) \ln(Q^{ss}(b)/Q^{ex}(b))$ [47]. The second measure of closeness is the *mean square error*: $(1/N)\sum_{b=1}^{N}[Q^{ex}(b) - Q^{ss}(b)]^2$, such that N spans over whole range of b of the experimental data. We have used these two quantities to study the data in Figs. 4(c) and 4(d) in the main manuscript. Their values (as reported in the main text) in these cases turned out to be quite low, indicating that theory matches well with experiments.

Denoting nth moment as $\mu_n = \langle b^n \rangle$, the respective moments of the theoretical and experimental distributions [in Figs. 4(c) and 4(d)] for the two synapses are compared in the table below.

	Synapse-1		Synapse-2	
	Theory	Experiment	Theory	Experiment
$\mu_2\|$	300	299	703	700
$\mu_3\|$	5508	5407	19 434	19 128
$\mu_4\|$	104 067	100 590	549 794	533 122

III: Here, we compare our theory with published data [39] and demonstrate estimation of a model parameter in the following way. For fixed ISI, the parameter p_{rb} associated with the binomial distribution is given by Eq. (12). Hence the mean quantal content $\langle b \rangle = M p_{rb}$ follows a particular dependence on the frequency of stimulation $f = 1/T$. Experimental data for $\langle b \rangle$ as a function of f is available from Ref. [39] for three different synapse types: two hippocampal (CA3-CA1 and EC-DG) and one auditory (MNTB-LSO). The evoked postsynaptic currents were converted to $\langle b \rangle$ using appropriate quantal sizes. For each of the three synapse types, the values of p_r

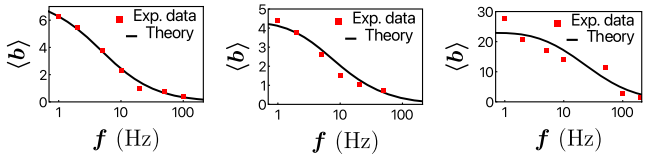

FIG. 5. The frequency dependence of the theoretical mean quantal content is matched with the experimental values for the synapse types (a) CA3-CA1, (b) EC-DG, and (c) MNTB-LSO. The parameters (given in Ref. [39], as well as estimated by our fit here) are as follows: (a) $M = 688$, $p_r = 0.011$, $k = 0.0523\ \mathrm{s}^{-1}$ (b) $M = 17$, $p_r = 0.251$, $k = 2.058\ \mathrm{s}^{-1}$ (c) $M = 147$, $p_r = 0.156$, $k = 3.816\ \mathrm{s}^{-1}$.

and the maximum vesicle docking rates kM are experimentally known [39]. Since we do not know the values of M and k separately, we do a one parameter fit with varying k to get the least square difference between the theoretical and experimental curves of $\langle b \rangle$ versus f. The best fit values estimated in this way of the model parameter $k = 0.0523\ \mathrm{s}^{-1}$, $2.058\ \mathrm{s}^{-1}$, and $3.816\ \mathrm{s}^{-1}$ respectively for the three neurons (see caption of Fig. 5 for values of M). The plots of the theoretical $\langle b \rangle$ with these estimated values (solid lines) are shown against the experimental data as a function of f. The extent of match validates Eqs. (11) and (12) for the frequency dependence of the mean quantal content in the steady state. At the same time, the procedure demonstrates a way of estimating the parameter k independently, which is hard using the formula for moments directly (see main text), for the constant ISI case.

*Corresponding author: ashok.prasad@colostate.edu
†Corresponding author: dibyendu@phy.iitb.ac.in

[1] S. Herculano-Houzel, Front. Hum. Neurosci. **3**, 31 (2009).
[2] Y. Tang, J. R. Nyengaard, D. M. De Groot, and H. J. Gundersen, Synapse **41**, 258 (2001).
[3] E. R. Kandel, J. Koester, S. Mack, and S. Siegelbaum, *Principles of Neural Science*, 6th ed. (McGraw Hill, New York, 2021), p. l, 1646.
[4] J. Del Castillo and B. Katz, J. Physiol. **124**, 560 (1954).
[5] V. N. Murthy and P. De Camilli, Annu. Rev. Neurosci. **26**, 701 (2003).
[6] S. O. Rizzoli and W. J. Betz, Nat. Rev. Neurosci. **6**, 57 (2005).
[7] A. A. Alabi and R. W. Tsien, Cold Spring Harbor Perspect. Biol. **4**, a013680 (2012).
[8] E. Neher, Neuron **87**, 1131 (2015).
[9] M. V. Tsodyks and H. Markram, Proc. Natl. Acad. Sci. U.S.A. **94**, 719 (1997).
[10] J. S. Dittman and W. G. Regehr, J. Neurosci. **18**, 6147 (1998).
[11] J. S. Dittman, A. C. Kreitzer, and W. G. Regehr, J. Neurosci. **20**, 1374 (2000).
[12] E. M. McLachlan, Int. Rev. Physiol. **17**, 49 (1978), https://pubmed.ncbi.nlm.nih.gov/29846/.
[13] S. Redman, Physiol. Rev. **70**, 165 (1990).
[14] A. Arleo, T. Nieus, M. Bezzi, A. d'Errico, E. d'Angelo, and O. J.-M. Coenen, Neural Comput. **22**, 2031 (2010).
[15] R. Rosenbaum, J. Rubin, and B. Doiron, PLoS Comput. Biol. **8**, e1002557 (2012).
[16] C. Pulido, F. F. Trigo, I. Llano, and A. Marty, Neuron **85**, 159 (2015).
[17] G. Malagon, T. Miki, I. Llano, E. Neher, and A. Marty, J. Neurosci. **36**, 4010 (2016).
[18] Z. Vahdat, Z. Xu, and A. Singh, in *2019 IEEE 58th Conference on Decision and Control (CDC)* (IEEE, New York, 2019), pp. 4729–4734.
[19] M. D. Miyamoto, J. Physiol. **250**, 121 (1975).
[20] R. Malinow and R. W. Tsien, Nature (London) **346**, 177 (1990).
[21] S. S. Kelly and N. Robbins, J. Physiol. **385**, 507 (1987).
[22] R. A. Silver, A. Momiyama, and S. G. Cull-Candy, J. Physiol. **510**, 881 (1998).
[23] H. Taschenberger, V. Scheuss, and E. Neher, J. Physiol. **568**, 513 (2005).
[24] C. Zhang and C. S. Peskin, Proc. Natl. Acad. Sci. U.S.A. **112**, 14954 (2015).
[25] C. Pulido and A. Marty, Physiol. Rev. **97**, 1403 (2017).
[26] C. D. Dürst, J. S. Wiegert, C. Schulze, N. Helassa, K. Török, and T. G. Oertner, Nat. Commun. **13**, 6126 (2022).
[27] Y. Hao, E. Toulmé, B. König, C. Rosenmund, and A. J. Plested, eLife **12**, e84029 (2023).
[28] E. Hanse and B. Gustafsson, J. Neurosci. **21**, 8362 (2001).
[29] C. Pulido and A. Marty, Physiol. Rev. **97**, 1403 (2017).
[30] G. Malagon, T. Miki, V. Tran, L. C. Gomez, and A. Marty, eLife **9**, e52137 (2020).
[31] A. Brémaud, D. C. West, and A. M. Thomson, Proc. Natl. Acad. Sci. U.S.A. **104**, 14134 (2007).
[32] H. Wen, M. J. McGinley, G. Mandel, and P. Brehm, Proc. Natl. Acad. Sci. U.S.A. **113**, E378 (2016).
[33] A. Barri, Y. Wang, D. Hansel, and G. Mongillo, eNeuro **3** (2016).
[34] A. D. Bird, M. J. Wall, and M. J. Richardson, Front. Comput. Neurosci. **10**, 116 (2016).
[35] O. Bykowska, C. Gontier, A.-L. Sax, D. W. Jia, M. L. Montero, A. D. Bird, C. Houghton, J.-P. Pfister, and R. P. Costa, Front. Synaptic Neurosci. **11**, 21 (2019).
[36] C. Gontier, S. C. Surace, and J.-P. Pfister, PLoS Comput. Biol. **19**, e1011342 (2023).
[37] S. Weis, R. Schneggenburger, and E. Neher, Biophys. J. **77**, 2418 (1999).
[38] K. Mahfooz, M. Singh, R. Renden, and J. F. Wesseling, PLoS Comput. Biol. **12**, e1004855 (2016).
[39] E. G. Krächan, A. U. Fischer, J. Franke, and E. Friauf, J. Physiol. **595**, 839 (2017).
[40] R. P. Costa, P. J. Sjöström, and M. C. Van Rossum, Front. Comput. Neurosci. **7**, 75 (2013).
[41] M. N. Shadlen and W. T. Newsome, J. Neurosci. **18**, 3870 (1998).
[42] G. Maimon and J. A. Assad, Neuron **62**, 426 (2009).
[43] See Supplemental Material at http://link.aps.org/supplemental/10.1103/PhysRevLett.132.228401, which includes Ref. [11], for comprehensive derivations of the analytical results, discussions on time dependent parameters,

correlated ISIs, and parameter estimation using simulated data.
[44] C. W. Gardiner, *Handbook of Stochastic Methods* (Springer, Berlin, 1985), Vol. 3.
[45] N. I. C. Müller, M. Sonntag, A. Maraslioglu, J. J. Hirtz, and E. Friauf, J. Physiol. **597**, 5469 (2019).
[46] N. I. C. Müller, I. Paulussen, L. N. Hofmann, J. O. Fisch, A. Singh, and E. Friauf, J. Physiol. **600**, 2461 (2022).
[47] L. Peliti and S. Pigolotti, *Stochastic Thermodynamics: An Introduction* (Princeton University Press, Princeton, 2021).
[48] R. Formisano, M. D. Mersha, J. Caplan, A. Singh, C. H. Rankin, N. Tavernarakis, and H. S. Dhillon, Synapse **74**, e22131 (2020).
[49] R. Formisano, K. D. Rosikon, A. Singh, and H. S. Dhillon, J. Neurosci. Res. **100**, 1551 (2022).
[50] J. S. Lee, W.-K. Ho, E. Neher, and S.-H. Lee, Proc. Natl. Acad. Sci. U.S.A. **110**, 15079 (2013).
[51] D. Keller, N. Babai, O. Kochubey, Y. Han, H. Markram, F. Schürmann, and R. Schneggenburger, PLoS Comput. Biol. **11**, e1004253 (2015).
[52] Y. Nakamura, H. Harada, N. Kamasawa, K. Matsui, J. S. Rothman, R. Shigemoto, R. A. Silver, D. A. DiGregorio, and T. Takahashi, Neuron **85**, 145 (2015).
[53] S. E. Brill, A. Maraslioglu, C. Kurz, F. Kramer, M. F. Fuhr, A. Singh, and E. Friauf, Front. Synaptic Neurosci. **12**, 560008 (2020).

Correction: The previously published Fig. 3(b) contained an error in the binomial curve and has been replaced.